

Resin Transfer molding of High-Fluidity Polyamide-6 with modified Glass-Fabric preforms

Gomez, Colin; Salvatori, Damiano; Caglar, Baris; Trigueira, Robin; Orange, Gilles; Michaud, Véronique

DOI

[10.1016/j.compositesa.2021.106448](https://doi.org/10.1016/j.compositesa.2021.106448)

Publication date

2021

Document Version

Final published version

Published in

Composites Part A: Applied Science and Manufacturing

Citation (APA)

Gomez, C., Salvatori, D., Caglar, B., Trigueira, R., Orange, G., & Michaud, V. (2021). Resin Transfer molding of High-Fluidity Polyamide-6 with modified Glass-Fabric preforms. *Composites Part A: Applied Science and Manufacturing*, 147, Article 106448. <https://doi.org/10.1016/j.compositesa.2021.106448>

Important note

To cite this publication, please use the final published version (if applicable). Please check the document version above.

Copyright

Other than for strictly personal use, it is not permitted to download, forward or distribute the text or part of it, without the consent of the author(s) and/or copyright holder(s), unless the work is under an open content license such as Creative Commons.

Takedown policy

Please contact us and provide details if you believe this document breaches copyrights. We will remove access to the work immediately and investigate your claim.



Resin Transfer molding of High-Fluidity Polyamide-6 with modified Glass-Fabric preforms

Colin Gomez^{a,1}, Damiano Salvatori^{a,1}, Baris Caglar^{a,b}, Robin Trigueira^a, Gilles Orange^c, Véronique Michaud^{a,*}

^a Laboratory for Processing of Advanced Composites, Ecole Polytechnique Fédérale de Lausanne, Station 12, 1015 Lausanne, Switzerland

^b Aerospace Manufacturing Technologies, Faculty of Aerospace Engineering, Delft University of Technology, Kluyverweg 1, Delft 2629HS, the Netherlands

^c Solvay Centre de Recherche de Lyon, 87 Avenue des Frères Perret, 69190 Saint-Fons, France

ARTICLE INFO

Keywords:

- A. Thermoplastic resin
- B. Polymer-matrix composites (PMCs)
- E. Resin transfer molding (RTM)
- E. Preforming

ABSTRACT

In Resin Transfer Molding (RTM), resin precursors of thermoset or, more recently, thermoplastic polymers are generally employed, raising issues related to the chemical reaction taking place during and after part processing. In this study, already polymerized polyamide-6 with low melt-viscosity (~ 30 Pa·s at 280 °C), is injected at low pressure (< 30 bar) in a custom-made mold, so as to impregnate glass fabric preforms via in-plane impregnation. Composite plates were produced using interply spacers acting as flow-enhancers. A three-step impregnation strategy, involving fast in-plane resin injection, a successive saturation step through transverse flow, followed by further micro-saturation caused by the collapse of the spacers, ensured industrially relevant impregnation kinetics. The influence of the spacer, the saturation time, pressure and temperature on the process kinetics and part quality were evaluated with three-point bending tests as well as microstructural analyses. Optimum processing parameters were identified and scaled up for a given part geometry.

1. Introduction

Resin Transfer Molding (RTM) process allows production of continuous fiber-reinforced polymer composite parts with relatively complex shapes by direct impregnation of a fabric preform compacted in a rigid mold cavity with a fluid resin prior to its consolidation/solidification. The resin is typically a reactive formulation of a thermoset (TS) resin, consisting in a mixture of a monomer and a curing agent that thermally initiates the polymerization reaction, which takes place in situ when full impregnation is achieved. TS resin precursors are widely used in composite manufacturing, as their low viscosity (0.01 to 1 Pa·s) ensures fast fabric impregnation. However, due to the physical properties of the matrix, thermoset composites exhibit low recyclability and workability, as well as low ductility and toughness.

For these reasons, in the past decades, efforts have been carried out in the scientific community to develop RTM using thermoplastic (TP) systems, consisting in injecting a reactive mixture of monomers/oligomers and activators/initiators, with subsequent in-situ polymerization [1,2]. The reactive thermoplastic systems include polyamide (PA) 6

[3–13] and 12 [14–19], poly(butylene terephthalate) (PBT) [20,21], and more recently PMMA [22–26]. Ideally, Resin Transfer Molding of Thermoplastics (TP-RTM) should combine the advantages of the thermoset RTM process (shape complexity, low waste, isothermal process) with those of a TP matrix (recyclability, workability, ductility, toughness). However, the in-situ polymerization reaction is difficult to control and may be affected by serious issues like concurrent crystallization or residual components (water, monomers, etc.) [5,27].

Recently, an alternative route has been conceived, thanks to the development of special grades of highly fluid engineering TPs (notably PAs) with melt viscosity in the range 10–100 Pa·s, which could be conveniently used to produce medium-size thermoplastic composite (TPC) components via RTM by direct impregnation of the reinforcing fabric from the melt state [28–37]. The matrix is provided as polymerized pellets, which are melt-processed to be injected in the hot RTM mold at low pressure/flowrate, and then cooled down to solidify the composite part. Compared to reactive TP-RTM, melt TP-RTM (or mTP-RTM) process would allow the production of TPCs in a well-controlled and repeatable way, using a conventional injection molding press. The

* Corresponding author.

E-mail address: veronique.michaud@epfl.ch (V. Michaud).

¹ Equal contributors

fluid velocity (melt polymer or resin) is typically modelled using Darcy's law, which allows predicting the time needed to fully impregnate a part of size L , along the flow direction. For example, for unidirectional saturated flow under constant fluid pressure at the mold inlet, impregnation time is found to be

$$t = \frac{\eta(1 - V_f)L^2}{2K\Delta P} \quad (1)$$

where η is the fluid viscosity, V_f is the fiber volume fraction, ΔP is the pressure difference between outlet and inlet, and K is the fabric permeability, a measure of how easily the fabric stack is impregnated by the melt polymer or resin, which depends on reinforcement properties (fiber volume fraction, fiber radius, fabric architecture). In order to reach high process cycle times (<10 min), it is necessary to optimize these parameters, taking into account the still relatively high viscosity of the polymer melt. A current solution is to inject the melt polymer transversally (reduce L) through the part thickness [34,37,38], which is typically in the order of few millimeters, i.e. approximately three orders of magnitude shorter than the part length. Even though transverse permeability of a fabric stack is generally lower than the in-plane one, the quadratic dependence on flow length (see Eq. (1)) makes this process faster, regardless of the part length. In addition, a higher pressure can be applied in compression RTM (C-RTM) up to 100 bar, with lower risk of fabric displacement. However, this process requires a mold with movable parts (mold and piston) with precise gaps and temperature control, coupled to a press and an injection molding machine, with the consequence of increasing the equipment cost and reducing the degree of complexity of the composite part compared to RTM, as no hollow or highly curved shapes can be easily conceived.

Another possible solution to reduce the processing time in Eq. (1), while keeping an RTM configuration (rigid mold, in-plane flow), is to increase the in-plane fabric permeability (K) by optimizing the preform architecture or to create flow channels [32,39–43]. Experiments performed on model fluids (stained aqueous solutions of PEG) and thermosets (epoxy resins) [42,43], have proven the efficiency of using spacers to create *meso*-channels in the preform and, as a consequence, increase its apparent permeability and shorten impregnation times. Furthermore, in these studies, permanent rigid spacers were used and acted as stiffeners, through a sandwich effect, in the composites, which increases part weight as compared to a foam structure. The spacer could also ideally collapse after impregnation to reach a uniform volume fraction. This approach has never been demonstrated so far for thermoplastic matrices, where the research gap is to develop collapsible composite spacers which survive the processing temperature (above 240 °C) and which adequately collapse after a small temperature rise, and to define a process route and conditions to reach shorter cycle times, as well as a well impregnated, good quality composite part. Eventually, this will result in guidelines to produce complex-shape parts (i.e. hollow shapes, highly curved and complex parts with integrated external features), with thermoplastics by RTM with commercially available textiles and polymer pellets, enabling post-forming and recycling possibilities. This in-plane RTM technique could be complementary to C-RTM that enables fast production of simpler shell-like geometries.

In this study, we thus investigate the benefits of using collapsible polymer interply spacers, acting as flow enhancers within glass fiber preforms, during mTP-RTM production of composite parts made of 2/2 twill woven glass fabrics and a high-fluidity melt polyamide-6 (HFPA6) thermoplastic. Experiments were performed on a lab-scale mold designed for this purpose under different processing conditions of applied pressure, saturation time and temperature with or without resin injection during the cooling phase. The resulting impregnation was evaluated by visual observation, optical microscopy, and mechanical performance in three-point bending tests. Finally, strategies were evaluated to further increase the overall kinetics of the process and to assess the possibility to reach industrially viable cycle times.

2. Experiments

2.1. Materials

A commercial, woven glass fabric under the brand name G-Weave™ was supplied by Chomarat (Le Cheylard, France). It is a balanced 2/2 twill with a total areal density of 600 g/m² and permeability of $(1.7 \pm 0.3) \times 10^{-10}$ m² at 45.8% fiber volume fraction, as measured in Ref. [41]. In parallel, an experimental stitched non-crimp fabric, called G-Ply™, with an areal density of 960 g/m² was used as a comparison element for flow kinetics only. This fabric features large *meso*-channels along the roll direction; the stitches are made of glass to allow high processing temperatures (>250 °C). Its permeability is in the range of 1 to 2×10^{-9} m² at 44.0% fiber volume fraction, as measured on a similarly built fabric in Ref. [41]. Both fabrics have been developed for thermoplastic composites and have a sizing compatible with a polyamide matrix.

HFPA6 under the brand name Evolite™ (XS1480) was supplied by Solvay in form of pellets containing a small quantity of additives (demolding agent, black pigment). Following supplier recommendations, a drying treatment at 110 °C overnight under low vacuum was performed on the pellets prior to use. Melt viscosity of HFPA6, which has a melting point of 223 °C, was measured on a rheometer AR2000ex (TA Instruments) in flow mode and plate-plate configuration, using aluminum plates of 25 mm diameter. Measurements were performed with constant shear rate of 1 s⁻¹ and at constant temperature of 240, 260 and 280 °C. The viscosity results are shown in Fig. 1, illustrating the low viscosity at elevated temperatures and a slight increase over time in air, which may be attributed to polycondensation of Nylon 6 occurring in dry conditions, i.e. for moisture content below the equilibrium point between hydrolysis and polycondensation [44].

Polyphenylene sulfide (PPS) filaments (Thermax PPS 3D) were supplied by 3DXTECH for the printing of spacers via Fused Deposition Modeling (FDM). PPS was selected as a model spacer material as it is available in a filament form for FDM with a glass transition temperature of 85 °C and melting point of 283 °C which makes it printable, yet, at the same time, structurally resistant for resin impregnation performed at temperatures up to 240–260 °C and collapsible upon elevation of temperatures during a post-impregnation step above its melting point. For mass production, a high temperature polyamide (PPA or PA6T/PA6I/PA6 for example) would be required, to be processed by injection molding and ensure a higher chemical compatibility with HFPA6 matrix. However, this material is not available for FDM processing.

Release agent XTEND W-4007 (Axel), suitable for high temperatures

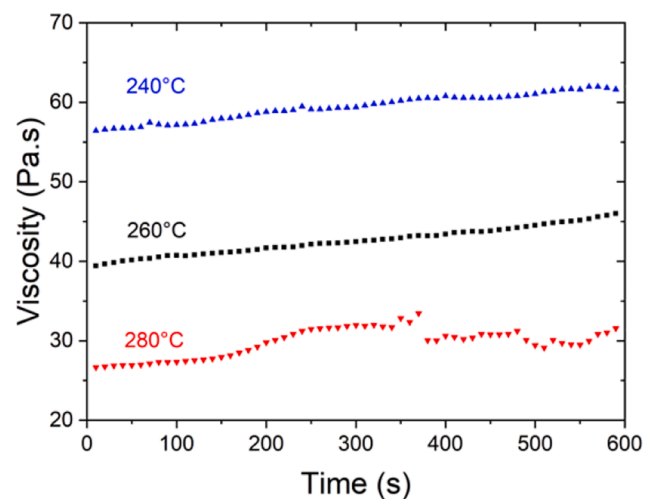


Fig. 1. Viscosity of HFPA6 from shear-flow rheology measurements at 1 s⁻¹ in air and at constant temperature.

(up to 500 °C), was used to ease material removal from the mold. Tacky Tape® sealant SM5160 (ITW Polymer Sealants North America), stable up to 400 °C, was used to minimize leakage from the mold.

2.2. Experimental setup

A custom-made tool was designed and manufactured for the production of small plates (7.5 cm × 11 cm) via in-plane mTP-RTM. The design concept is schematically shown in Fig. 2. A compact design was conceived, so as to minimize equipment cost and complexity, and avoid the use of an injection molding press (which is an ideal candidate for an industrialization scale up). The tool was entirely machined in steel and its surface hardened by nitriding treatment. It embodies a molding cavity and two pots for pellet melting, to allow injecting the melted polymer from either one or both gates. However, for the purpose of this study, the melt was fed into the mold from a single cavity. The piston compresses the fluid (melt) to squeeze out the air and injects the melt polymer to the underlying cavity through a hole (inlet) of 3 mm diameter, with manual opening/closing control by a screw. In addition, a vacuum-pump is connected to the outlet gate, in order to evacuate air from the cavity. The tool is operated with a hydraulic hot press (Fontjine Press, maximum force 60 kN), which provides a heating source from both top and bottom. The injection of resin is ensured by a closing force applied by the upper part of the press on the piston with a surface area of 3090 mm², used to convert the nominal force into a resin pressure. Additional heating is locally provided by three heating cartridges (800 W each) of diameter of 1 cm, each individually controlled by a thermocouple, inserted in the middle plate. The heating system of the press is used to reach the different temperatures related to the process steps and the mold temperature is monitored with additional thermocouples both below the molding cavity and at the melting pot.

2.3. Production of polymer spacers

PPS spacers were designed to create *meso*-channels that are 6 mm wide and 2 ± 0.1 mm high, as shown in Fig. 3a, 3b and 3c. These beams of 0.25 mm high connected the longitudinal beams each 25 mm. These spacers were printed in a single part at a temperature of 340 °C using an AON 3D printer, based on the design as proposed in Ref. [42], but simplified to allow for easier printing of the part with PPS material. Prior to printing, the PPS filaments were dried overnight in an oven at 110 °C. The spacing was designed to reach a high permeability of the channel while resisting the pressure imposed by the compressed fabric at the impregnation temperature. A first assessment was carried out by

compaction tests of the fabric stacks at room temperature to estimate the average compaction pressure exerted by the fabric, which was about 1.5 MPa on a strut. Thermomechanical tests in three-point bending were then performed on PPS 3D printed flat rectangular samples, under a static force of 3.2 N to simulate the compaction pressure of 1.5 MPa exerted by the fabric, with a temperature ramp from 40 to 300 °C. As the T_g of PPS is 85 °C, we particularly observed the sample deflection above this temperature up to the injection temperature of 240 °C. Results indicated a slightly increased deflection above 100 °C for all samples, but which remained limited. For the as-produced samples, a larger deflection was observed when the sample reached 200 °C. This could be well mitigated by increasing the crystallinity of the PPS through an annealing stage to increase its crystallinity, the best result was obtained for a sample annealed at 240 °C, where the deflection remained stable until about 250 °C. For all samples, complete collapse was observed as expected when the temperature reached 283 °C, melting point of the polymer. From these preliminary experiments, it was thus found necessary to anneal the PPS spacers at 240 °C for 3 h to reach a crystallinity above 60% and Young's modulus above 3 GPa, following recommendations from Ref. [45], and thus to minimize spacer premature collapse until impregnation takes place.

The preliminary assessment of the PPS spacers was validated by the preparation of mock samples, whereby the spacer and fabrics were subjected to the desired processing temperature cycle without PA impregnation, then cooled down and impregnated with mounting epoxy resin so as to keep the structure, demolded and inspected. A cross section of a mock sample which underwent the process cycle up to 240 °C only is presented in Fig. 3a, confirming that the spacer did not collapse at this temperature. The fabric is observed to relax partially between the spacer struts, which is expected to influence the channel permeability, nonetheless large triangular channels are still present. Another mock sample was performed, with the process cycle up to 290 °C for 10 min, also presented in Fig. 3(a). The PPS spacer was well collapsed close to the heating cartridges (as shown in the figure), and partially collapsed in between. As a result, the second temperature dwell necessary to ensure complete melting and collapse of the spacer material in the following experiments was set to 300 °C for 5 min.

2.4. Production of composites

G-Weave fabrics were manually cut with a roll-cutter to rectangles of 7.5 cm × 11 cm in size. Ten plies were laid up with the same orientation; between the fifth and sixth plies a spacer was introduced. In all experiments, the cavity thickness was set to 5 mm, which led to an overall

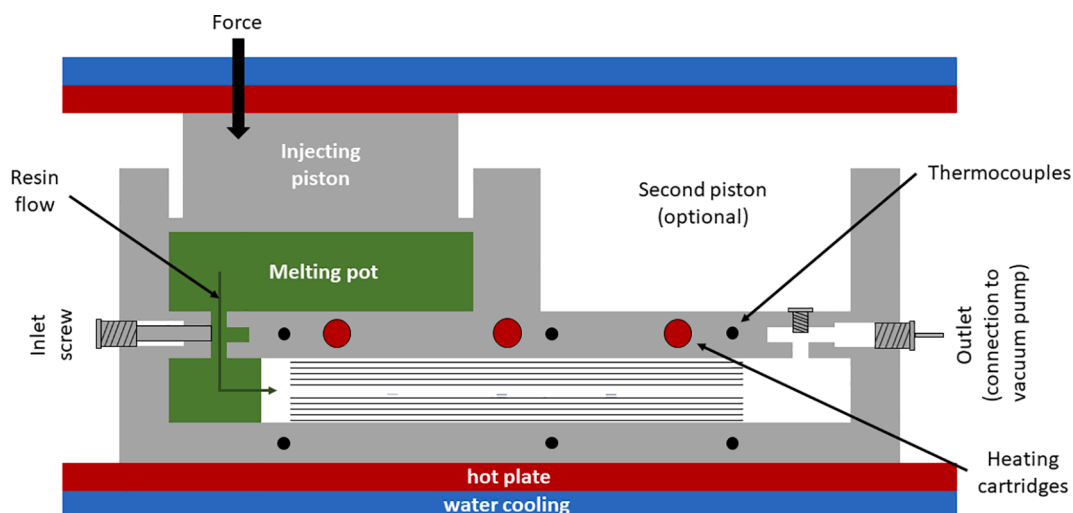


Fig. 2. Schematic cross-sectional side view of the experimental set-up placed in the press.

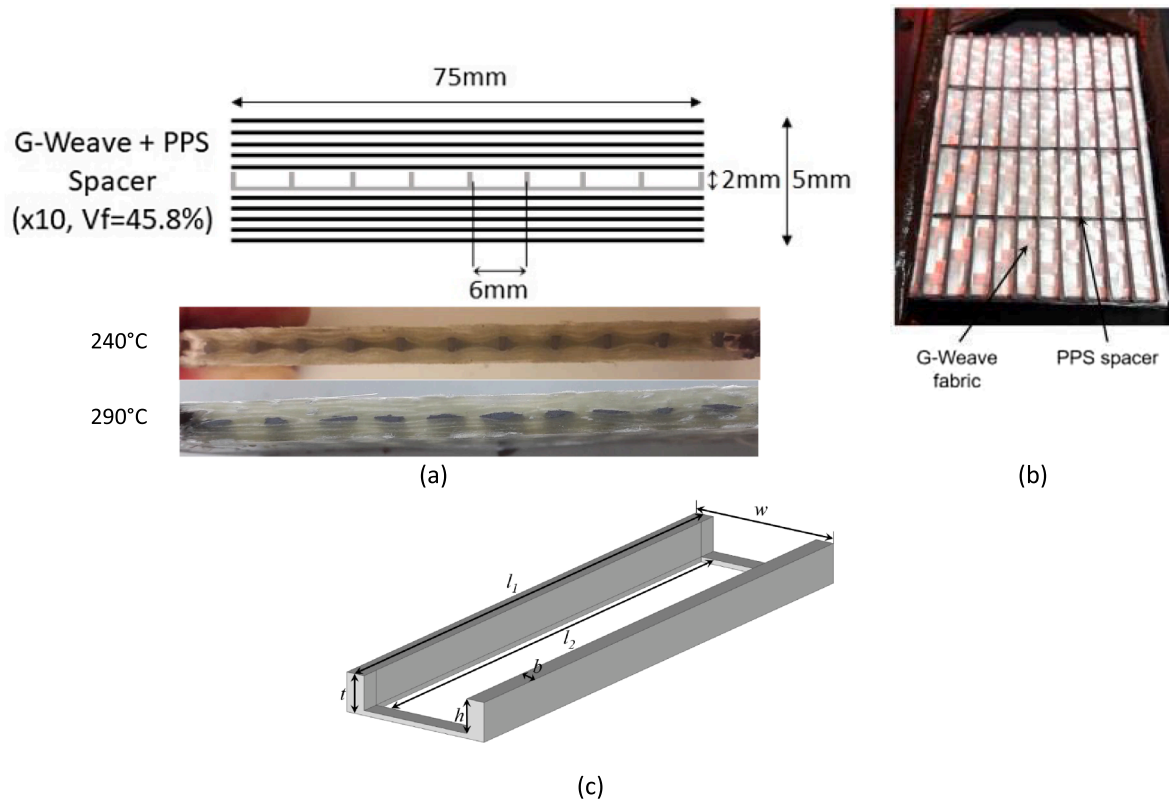


Fig. 3. Schematic cross-sectional view of the G-Weave+Spacer lay-up (transversal view with respect to the flow direction), as well as cross-section of the mock samples (a), picture of the spacer placed on top of the fifth layer of fibers (b) and unit cell of the spacer grid. ($l_1 = 27$ mm, $l_2 = 25$ mm, $t = 2$ mm, $h = 1.75$ mm, $b = 1$ mm and $w = 8$ mm) (c).

glass fiber volume fraction of 45.8% (calculated from the areal weight of the fabric, the number of plies and their dimensions as well as the cavity thickness of 5 mm). The variations in the total fabric lay-up weight (± 0.50 g for an average weight of 51.04 g) led to a variation of the fiber volume fraction of $\pm 0.46\%$ between plates. Note that the volume fraction was limited by the presence of the spacer, which led to an additional compaction of the fiber bed. Indeed, on top of and below the spacer, i.e. in the regions where the fiber plies were compacted, the fiber volume fraction was calculated to reach up to 76.4%. As references, two plain plates were produced without any spacer in their structure. The first one is made of the same lay-up sequence of G-Weave and the second plate is made of 6 plies of G-Ply fabric all laid-up with the *meso*-channels oriented in the in-plane flow direction (see Fig. 4). It led to a total fiber volume fraction of 44.0%.

In a typical impregnation test, the sandwich, made out of the glass fabrics and the spacer, is first placed in the cavity, the mold is then assembled and closed before polymer pellets are poured into the melting pot. The mold is then placed in the press and vacuum is pulled out of the cavity containing the preform, using a vacuum pump connected to the outlet. Then, heating from both the press platens and the cartridges is

activated. At the same time, a low pressure is applied on the pellets to increase heat conduction in the pellet cavity. During heating, the inlet gate is first opened to evacuate the remaining air bubbles present in the pellets, thanks to the connected vacuum system. When the mold temperature approaches the melting point of the pellets, the inlet gate is closed to avoid a premature injection of the resin in the cavity, and the melt gets squeezed in the melting pot. When the temperature both at the melting pot and the cavity reaches the desired temperature, typically between 240 and 260 °C depending on the experiment, the inlet is opened and impregnation starts. As a first step, the resin follows a fast in-plane flow through the *meso*-channels of the spacer. This step is called “injection”. Once the resin reaches the outlet gate, this latter gets instantly clogged by solidification of the melt, since the temperature of the outlet gate is significantly lower than the melting point of the resin (preventing the rest of the resin from flowing through this gate for the rest of the process) and the vacuum pump is turned off. At this instant the second step (called “saturation”) starts, maintaining resin injection for the desired period of time (“saturation time”), to force the resin to impregnate the preform in the through-thickness direction. These two steps are represented schematically in Fig. 5. The injection pressure was kept constant for all experiments to 3.6 bar, however the saturation pressure was part of the studied parameters. Its increase is monitored by the force applied by the press on the piston. Then the press, and cartridges, temperature is increased up to 300–305 °C (above PPS’ melting point) and the temperature is kept constant for a pre-determined duration (typically 5 min) for the spacer to collapse. During the spacer collapse, the compaction stresses applied on the fiber stacks relax, further enhancing through thickness impregnation. Finally, the cartridges are switched off and cooling, from both above and below the mold, is activated. Due to the design of the setup, the cavity is closer to the bottom cooling plate than the top one (as depicted in Fig. 2), inducing a directional solidification from the bottom of the mold to the

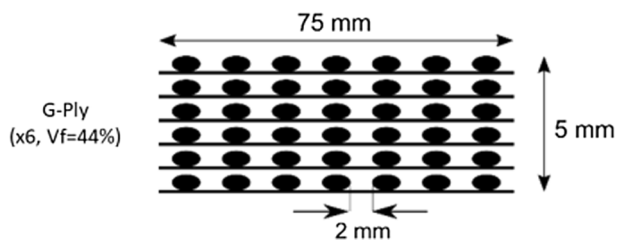


Fig. 4. Schematic cross-sectional view of the G-Ply lay-up (transversal view with respect to the flow direction).

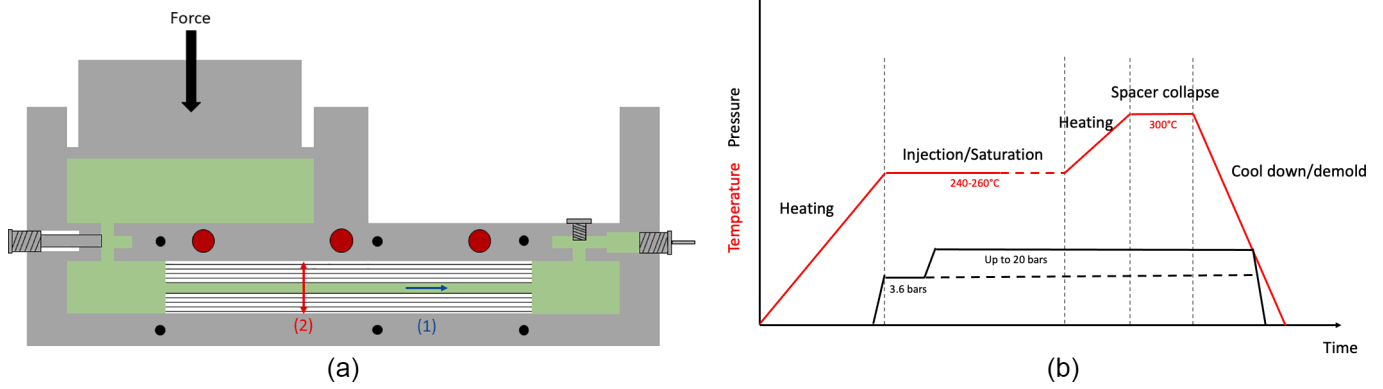


Fig. 5. (a) Schematic of the two-steps impregnation strategy, with (1) the injection step and (2) the saturation step. (b) Schematic of the impregnation temperature and pressure profile versus time during an experiment.

top. During the collapsing phase of the spacer and the cooling of the mold, the inlet is kept either opened or closed (to maintain or stop resin injection), this is another parameter of this study.

The different plates, with their corresponding processing conditions and mechanical characteristics, are gathered in Table 1. In general, one plate was produced per combination of conditions, and repeats were

performed for some of the plates to check reproducibility. All plates had a thickness comprised between 4.9 and 5 mm, with an average at 4.96 mm, as imposed by the cavity thickness.

Table 1

Processing parameters for the different plates manufactured, their corresponding bending properties and void fraction.

Comparison parameter	Plate N°	Spacer	Injection Pressure [bar]	Injection Temperature [°C]	Saturation Time [s]	Saturation Pressure [bar]	Saturation Temperature [°C]	Feeding	Average Bending Strength (±SD) [MPa]	Average Flexural Modulus (±SD) [GPa]	Void Fraction (±SD) [%]
References	A	No	3.6	240	/	/	/	/	/	/	/
	B (G-Ply)	No	3.6	240	1200	10	240	Yes	/	/	/
Saturation Pressure	4	Yes	3.6	240	600	3.6	240	Yes	310.0 ± 13.8	16.5 ± 0.6	4.28 ± 1.9
	13	Yes	3.6	240	600	10	240	Yes	353.8 ± 81.4	19.3 ± 1.7	2.46 ± 0.9
	22	Yes	3.6	240	600	15	240	Yes	407.9 ± 61.1	17.6 ± 1.8	2.24 ± 0.7
	20	Yes	3.6	240	600	20	240	Yes	431.9 ± 11.4	17.7 ± 1.5	1.08 ± 0.3
Saturation Time	5	Yes	3.6	240	300	3.6	240	Yes	311.5 ± 68.4	16.8 ± 0.9	7.05 ± 1.6
	4	Yes	3.6	240	600	3.6	240	Yes	310.0 ± 13.8	16.5 ± 0.6	4.28 ± 1.9
	13	Yes	3.6	240	600	10	240	Yes	353.8 ± 81.4	19.3 ± 1.7	2.46 ± 0.9
	21	Yes	3.6	240	1200	10	240	Yes	375.5 ± 61.6	18.4 ± 0.5	3.26 ± 1.5
	6	Yes	3.6	240	600	3.6	240	No	254.1 ± 35.1	15.6 ± 0.8	7.43 ± 2.9
Feeding	9	Yes	3.6	240	900	3.6	240	No	326.4 ± 11.0	16.2 ± 0.2	3.6 ± 1.1
	4	Yes	3.6	240	600	3.6	240	Yes	310.0 ± 13.8	16.5 ± 0.6	4.28 ± 1.9
	6	Yes	3.6	240	600	3.6	240	No	254.1 ± 35.1	15.6 ± 0.8	7.43 ± 2.9
	7	Yes	3.6	240	600	10	240	No	233.0 ± 5.0	15.3 ± 0.2	6.09 ± 3.2
	13	Yes	3.6	240	600	10	240	Yes	353.8 ± 81.4	19.3 ± 1.7	2.46 ± 0.9
Injection and saturation temperature	16	Yes	3.6	260	1200	10	260	Yes	438.5 ± 61.6	19.4 ± 0.5	1.2 ± 1.1
	23	Yes	3.6	250	1200	10	250	Yes	424.6 ± 37.7	18.9 ± 0.6	2.06 ± 1.7
	21	Yes	3.6	240	1200	10	240	Yes	375.5 ± 43.3	18.4 ± 1.3	3.26 ± 1.5
Tests optimum	14	Yes	3.6	240	900 (600/300)	10/15	240	Yes	459.8 ± 19.0	18.4 ± 0.5	2.95 ± 0.6
	18	Yes	3.6	240	1200 (600/300/300)	7/10/15	240	Yes	471.8 ± 36.5	19.0 ± 0.6	0.77 ± 0.5

2.5. Composite analysis

Composite samples were cut with a diamond blade, as depicted in Fig. 6, from the produced plates in order to perform microstructural observation and three-point bending tests for assessment of the mechanical properties in the flexural mode. Samples, of approximately 13x13 mm in size, were cut from three different locations along the impregnation direction: close to the inlet, the center of the plate and close to the outlet (see Fig. 6). These samples were analyzed via optical microscopy to assess the void content at the micro-scale of the cross sections both along and transverse to the flow direction. An automated polishing machine (Struers), in combination with SiC papers, was used to polish the samples for microscopic observations with a Keyence microscope (VHX-S550E base, OP-88164 lighting head and VH-Z100R lens at magnifications from 100x to 200x).

The ASTM D7264 standard for three-point bending tests on polymer matrix composites was used as a reference for sample preparation and for bending modulus, E_f , and flexural strength, σ_{max} , measurements [46]. Three beams with length of 10 cm and width of 13 mm were cut from each plate along the flow direction, at three different locations (see Fig. 6). These samples were cut using a diamond saw mounted on a Maiko cutting machine and polished afterwards. Flexural tests were carried out in a mechanical testing machine (Walter + Bai AG Series LFL-125kN) using a span-length of 6 cm for all the tests, resulting in a span-length-to-thickness ratio of 12:1. Note that this span to thickness ratio is below the minimal value recommended by the standard for pure flexural tests, as we were limited by the dimensions of the mold. We thus expect a shear contribution of about 4%, which remains acceptable, considering that the measurements are mainly performed to compare samples made with different process parameters, but with the same geometry. Displacement speed was set to 1 mm/min and a load-cell of 10 kN was used for force measurement. In all tests, samples were positioned with the same side facing up, so any potential variation due to asymmetry of the mold cooling rate was not assessed in this work.

From force-displacement data, flexural stress (σ) and strain (ϵ) on specimen tensile face were obtained using the following equations:

$$\sigma = \frac{3FL}{2bh^2} \quad (2a)$$

$$\epsilon = \frac{6\delta h}{L^2} \quad (2b)$$

where F is the applied force, L the span-length, δ the mid-span deflection, and b and h the width and the thickness of the sample, respectively, which were measured for each sample. The flexural modulus was defined as the slope of the stress-strain curve between 0.001 and 0.003 of strain, and bending strength as the maximum stress attained.

Void content measurements, performed on the four cross-sectional faces of the (13 × 13) mm² samples located close to the outlet, were carried out by image analysis on the micrographs. Color micrographs were converted into grayscale images, then into binary images using thresholding and size filters to isolate areas corresponding to the pores. The void content was calculated as the ratio between the total area of the pores and the total area of the observed cross-section.

3. Results and discussion

3.1. Flow enhancement by use of a spacer

The injection time was defined as the necessary time for the resin to reach the outlet. It was measured from the moment the inlet was opened for injection until the moment the resin flew through the outlet gate (visual tracking was not possible due to the metallic mold halves). Thus, these durations included the times during which the resin flowed from the inlet to the beginning of the preform and from the end of the preform to the outlet (a few cm each). For injections performed at 240 °C, the average injection time was 61 s (±16 s). The variation in the injection time is attributed to experimental variations in the preform arising from nesting between the spacer and fabric yarns, or small variations in the spacer's height, as well as the variability in melt viscosity due to temperature fluctuations during the injection (240 °C ± 3 °C). For the injections performed at 260 °C the injection time was 110 s (±22 s). The injection time can be calculated from Eq.(1), estimating the overall preform permeability using the hydraulic resistance for a representative channel, as shown in our previous studies, assuming that the contribution of micro-flow can be neglected [41,42]. The (saturated) permeability of a preform embodying an array of channels of perimeter P_c , area A_c , and cross-sectional unit-area per channel A is thus given as:

$$K_{\text{meso-channel}} = \frac{A_c^3}{2P_c^2 A} \quad (3)$$

Considering isosceles triangular channels as observed in Fig. 3a, of base 1.75 mm and height 3 mm (a half channel size), in a channel of 3 mm width and 5 mm height, $K_{\text{meso-channel}} = 8 \times 10^{-9} \text{ m}^2$, which is close to the permeability of a similar construction measured in Ref. [42], of $1 \times 10^{-8} \text{ m}^2$. At 240 °C, Darcy's law thus predicts, for an 11 cm long composite construction of this type, an injection time of 68 s, which is in good agreement with the observed data. At 260 °C, injection time is predicted to 48 s assuming the same permeability, as the viscosity is lower at this temperature. The increased injection times at 260 °C is thus attributed to a partial collapse of the PPS spacer as a consequence of the compaction stress applied by the fabric at a temperature closer to its melting point (of 283 °C). Thus, 240 °C seems to be the optimal impregnation temperature for this spacer construction, although up to 260 °C is still possible, albeit with a reduction in impregnation speed.

As a comparison, the impregnation of a fabric-only configuration performed on G-Weave fabric at 240 °C resulted in an incomplete impregnation after 1 h and 10 min, as shown in Fig. 7 (more than 70 times longer than the injection time for the same composite with the spacer), verifying the two orders of magnitude of improvement in flow kinetics expected from the spacer. Darcy's law foresees an injection time of 54 min at this temperature.

Impregnation of G-Ply fabrics at the same conditions (i.e. temperature and injection pressure) took 3 min and 59 s, four times more than

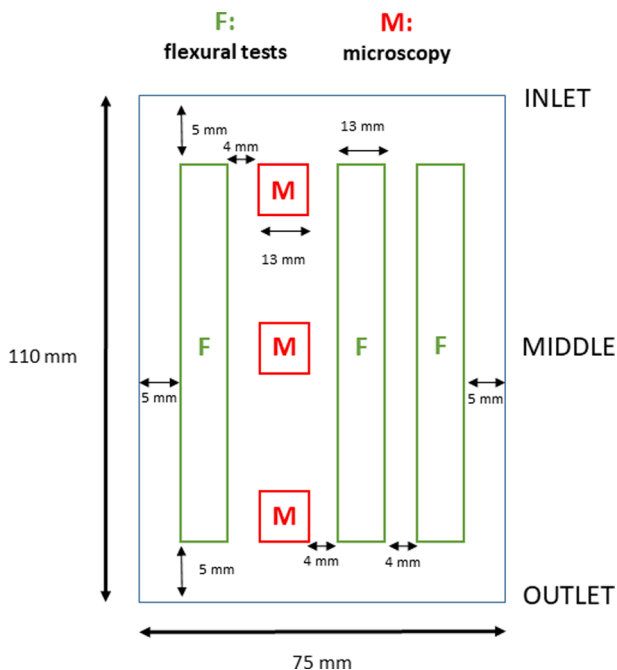


Fig. 6. Schematic top view of the samples cut off the plates.



Fig. 7. Macroscopic view of the G-Weave plate impregnated at 240 °C without spacer.

for the G-Weave with spacer, but without the need for a saturation phase; the part was completely impregnated, as shown in Fig. 8, in accordance with the fill time prediction obtained using Eq. (1) and permeability characteristics reported in Ref. [41]. This route is thus viable; however, this fabric is not commercially available (as it is specially designed with glass stitches) and the large channels, made to increase its permeability, remain in the final part, leading to potential inhomogeneity issues.

Thus, channel permeability is clearly the discriminating factor between these samples manufactured at similar pressures (3.6 bar), temperatures (240 °C) and fiber volume fractions (44.0% and 45.8%) with the same dimensions. The specially designed spacers enabled shorter

injection times compared to the composites without spacers or with *meso*-channels in their fabric architecture, in agreement with our previous results on model systems with epoxy matrix [42]. These results also show the ability of the spacer to maintain its role at temperatures up to 260 °C, however with the need to keep a margin for the injection temperature with regards to the melting point of the spacer.

3.2. Effects of saturation pressure

After injecting the resin (“injection phase”) at 3.6 bar, the specimens underwent different saturation pressures during the saturation phase (see Table 1). Results for the mean bending strength and flexural modulus at each pressure are shown in Fig. 9.

An increase in the bending strength was observed at higher saturation pressures (ranging between 3.6 bar and 20 bar), from (310.0 ± 13.8) MPa at 3.6 bar to (431.9 ± 11.4) MPa at 20 bar which represents an increase of 39.3%. This was expected as a higher pressure enhances resin transverse impregnation into the glass fabrics, which were initially compressed to high volume fraction. Flexural moduli are all observed to be within the same range, considering standard deviation, between (16.5 ± 0.6) and (17.7 ± 1.5) GPa, hence not affected by the saturation

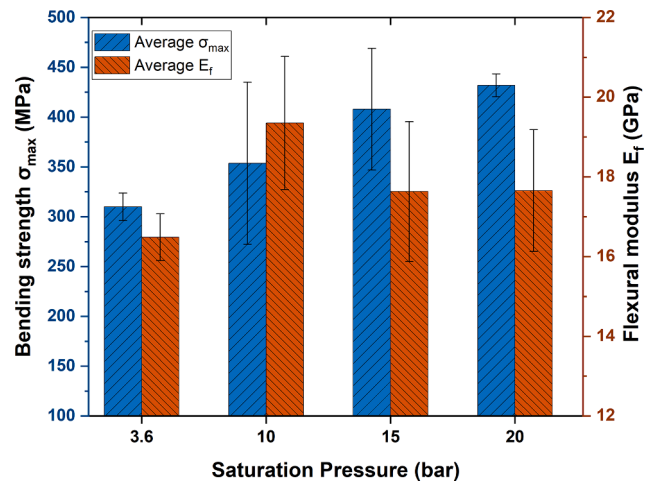


Fig. 9. Bending strength and modulus as a function of the saturation pressure. (Feeding ON, 10 min saturation and injection at 240 °C for all samples).



(a)



(b)

Fig. 8. G-Ply lay-up before (a) and after (b) impregnation.

pressure level. According to laminate theory, this value was expected for a 45.8% fiber volume fraction composite made of 2/2 twill (0/90°) E glass fabrics, with fibers of approximately 70 GPa of modulus. The microstructural analyses performed on these samples showed a good correlation between the void content and the mechanical properties detailed above. Indeed, a reduction in the void content from 4.28% at 3.6 bar to 1.08% at 20 bar was observed (see Table 1). These effects are illustrated in Fig. 10.

It is important to note that some fiber misalignment was observed on the upper surface of the plates saturated above 10 bar. It was attributed to the fast increase in pressure after the injection phase. During injection, resin flows preferentially first through the spacer and does not impregnate the top and bottom fiber plies, which thus remain dry. When the pressure is suddenly increased for the saturation phase, the resin gets in contact with dry fibers, at high speed, on the top and bottom faces of the preform, dragging them with it. This type of artefact may have critical consequences for parts that may experience tensile loads; thus, complementary tensile tests should be performed on these samples. A potential solution, tested on longer saturation times, consisting in a gradual increase in pressure, with a short plateau after each increment, (instead of an increase in a single shot) showed good results in reducing fiber misalignment.

3.3. Effects of saturation time

The effects of saturation time on the impregnation quality and the flexural properties were investigated with three different processing conditions as reported in Table 1. When resin injection was maintained during the collapsing phase of the spacer and during cooling (Fig. 11. a and b) the effects of the saturation time on the bending strength and bending modulus are negligible, as the variations range in the interval of the standard deviations. However, in the cases where impregnation was stopped after the saturation phase, the saturation time affected the bending strength. Indeed, the bending strength increases by 28.5% when the saturation time is extended from 600 s to 900 s (see Fig. 12). Void content follows the same trend with a drop from 7.43% to 3.60% for saturation times of 600 s and 900 s, respectively. Moreover, the

homogeneity of the results is improved, both for the stress and the modulus, when the saturation time is increased. This is explained by a more homogeneous distribution of the melt along the thickness when the saturation time increases. For those samples where feeding was not maintained during the cooling phase, a longer saturation time also ensures a higher saturation of the fabric by the resin, which partially compensates the effect of crystallization shrinkage taking place during the cooling phase. A more detailed analysis of this phenomenon is studied in the section below.

Finally, these last results are in accordance with the optical micrographs shown in Fig. 13.

3.4. Effects of resin feed during crystallization

Polyamide being subject to crystallization shrinkage [49], some experiments were conducted to evaluate to which extent crystallization conditions might affect the impregnation quality of the specimens. To do so, resin injection was stopped after the saturation phase (i.e. before the collapsing phase of the spacer and the cooling of the mold) (namely “feeding OFF”) and results of the mechanical tests and micrographs were compared with those of plates for which resin injection was maintained until the end of the process (namely “feeding ON”). These tests were conducted at two different pressures (3.6 bar and 10 bar) and had similar effects on the flexural properties of the produced plates. As shown on Fig. 14, both the bending strength and flexural modulus increased when resin injection was maintained until the end of the process. The bending strength increased by 22.0% and 51.8% at saturation pressure of 3.6 bar and 10 bar, respectively. The lower results, obtained when the feeding was turned off, highlight the effect of crystallization shrinkage that is further amplified by the directional cooling. By design, the lower part of the mold cools down faster. As a consequence, crystallization starts from the lower side of the part and the remaining melted matrix above flows down to fill the porosities created by the shrinkage. If the resin injection is maintained during this period, the displaced polymer is replaced by the polymer fed through the inlet. However, when feeding is turned off the shrinkage generates porosities which cannot be entirely fed by the material above. As a result, all

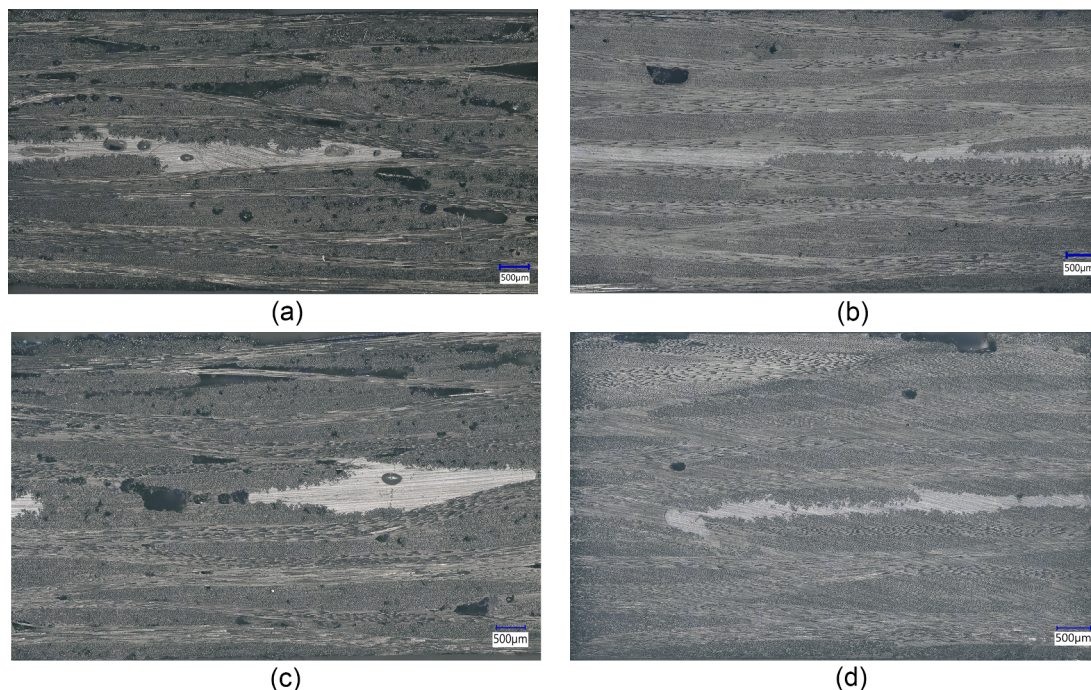


Fig. 10. Optical micrographs of samples cut close to the outlet, longitudinally (a and b) and transversally (c and d) to the resin flow; for saturation pressures of 3,6 bar (a and c) and 20 bar (b and d). (Feeding ON, 10 min saturation and injection at 240 °C for all samples).

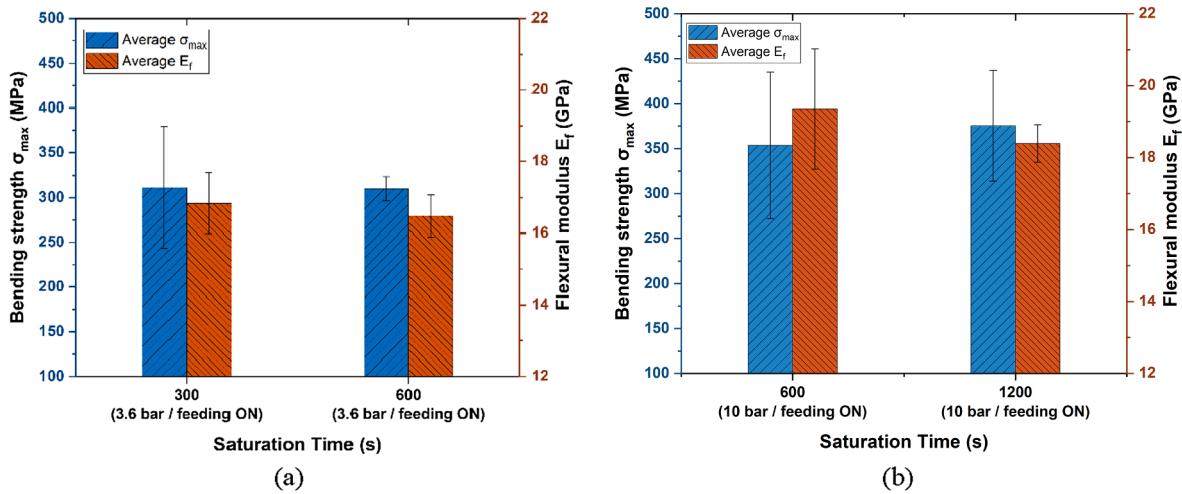


Fig. 11. Bending strength and bending modulus as a function of the saturation time; for saturation pressures of 3,6 bar (a) and 10 bar (b). ("feeding ON": resin injection was maintained during spacer collapse and polymer crystallization). (Injection at 240 °C).

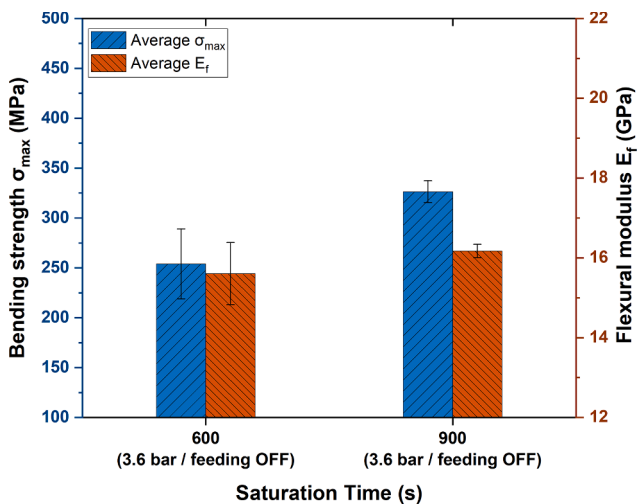


Fig. 12. Bending strength and bending modulus as a function of the saturation time; with a saturation pressure of 3,6 bar. ("feeding OFF": resin injection was stopped before spacer collapse and polymer crystallization). (Injection at 240 °C).

samples exhibit porosities on the upper half of the samples whereas only some of them have porosities on the lower half of the micrographs (see differences between Fig. 15. a-c and Fig. 15 b-d) that ultimately results in lower flexural properties.

Void content analyses also revealed an important reduction in porosity content when melt feeding was maintained until the end of the process. The void content was reduced by 42.4% (from 7.43% to 4.28%) and by 59.6% (from 6.09% to 2.46%) at saturation pressure of 3.6 bar and 10 bar, respectively.

3.5. Effects of injection and saturation temperature

Three injection and saturation temperatures were tested, namely 240, 250 and 260 °C. The melting temperature of PPS being 283 °C and the spacer being compressed between the two stacks of glass fibers, the injection temperature was not raised above 260 °C to avoid a premature collapse of the spacer during the injection or saturation phase. Fig. 16 shows a slight increase in the bending strength when the temperature is raised, of the order of 16.8% from 240 to 260 °C. The void content also decreases, from 3.26% to 1.20%, when the temperature is increased.

This can be attributed to the lower viscosity of the polymer with increasing temperature, as shown in Fig. 1, leading to an improved impregnation of the micro-cavities and intra-bundle spaces. Another factor may relate to a more favorable balance between viscous and capillary effects at higher temperature, due to a lower capillary number Ca, which is the ratio of fluid velocity times viscosity over surface tension [50,51].

3.6. Optimal processing parameters

Based on the conclusions drawn from the above detailed experiments, additional tests were performed to obtain plates with higher mechanical properties and lower porosity contents, by adjusting the processing conditions. The processing parameters for those samples were compared with the trends observed for each individual parameter, as studied in the different sections above; the optimum parameters are gathered in Table 2. The corresponding micrographs are shown in Fig. 17. The bending strength reached values as high as 471.8 MPa and the bending modulus ranged around 19 GPa, while the volume fraction fibers was the same as for all previous samples. The micrographs, captured on samples cut close to the outlet of the plate, revealed a low void content, in comparison with the other manufactured plates.

Furthermore, the processing parameters for those parts are in accordance with the optimal ones identified in the above sections; namely: feeding ON during spacer's collapse and matrix crystallization and a saturation pressure between 10 and 15 bar (with a gradual increase).

3.7. Towards a scale-up in automotive applications

With the aim to evaluate potential scaling up of this new mTP-RTM technique to industrial applications with large production volumes, a rectangular plate, with dimensions similar to that of a car bonnet (1.5 m × 1.6 m), was considered. Three different inlet configurations were considered as shown in Fig. 18: a single inlet (similar to the experimental one detailed above), a double inlet (with an additional inlet gate placed at the other end of the part) and a peripheral system (the resin being injected from all around the part simultaneously, considering that the spacer design is also adapted for peripheral injection). Three different injection temperatures (240, 260 and 280 °C) were considered and the injection times were calculated for all the temperature – inlet configuration combinations. The saturation times are assumed to remain the same for all cases as saturation takes place as transverse impregnation after injection is finished. The same fiber volume fraction as above

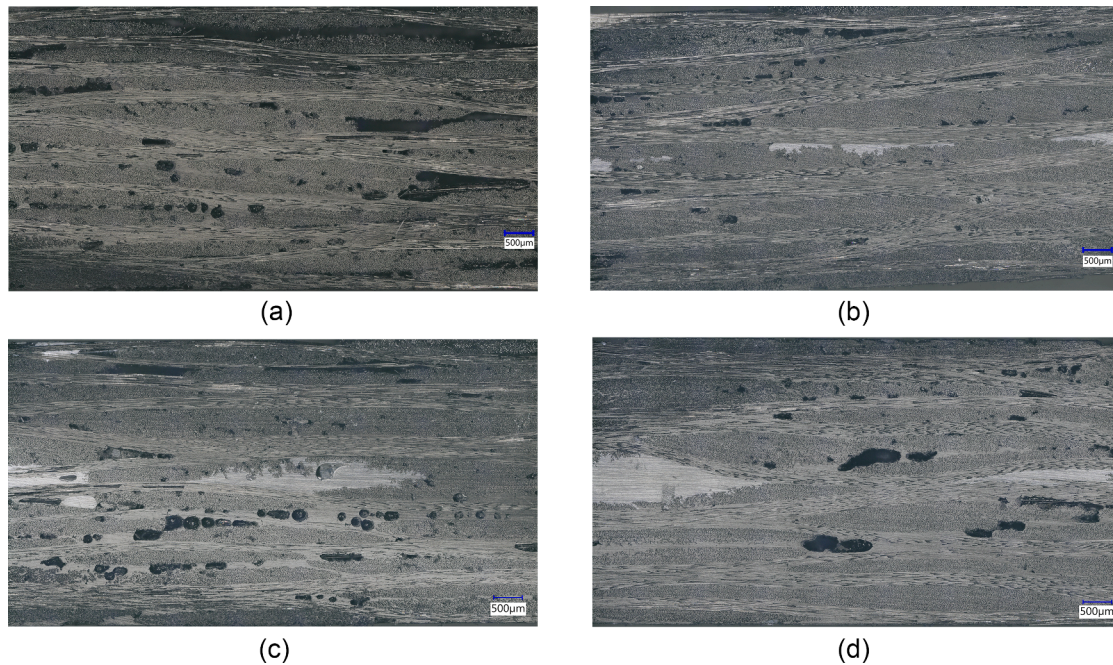


Fig. 13. Optical micrographs of samples cut close to the outlet, longitudinally (a and b) and transversally (c and d) to the resin flow; for saturation times of 600 (a and c) and 900 (b and d) s. (Saturation pressure: 3,6 bar, Feeding OFF and Injection at 240 °C).

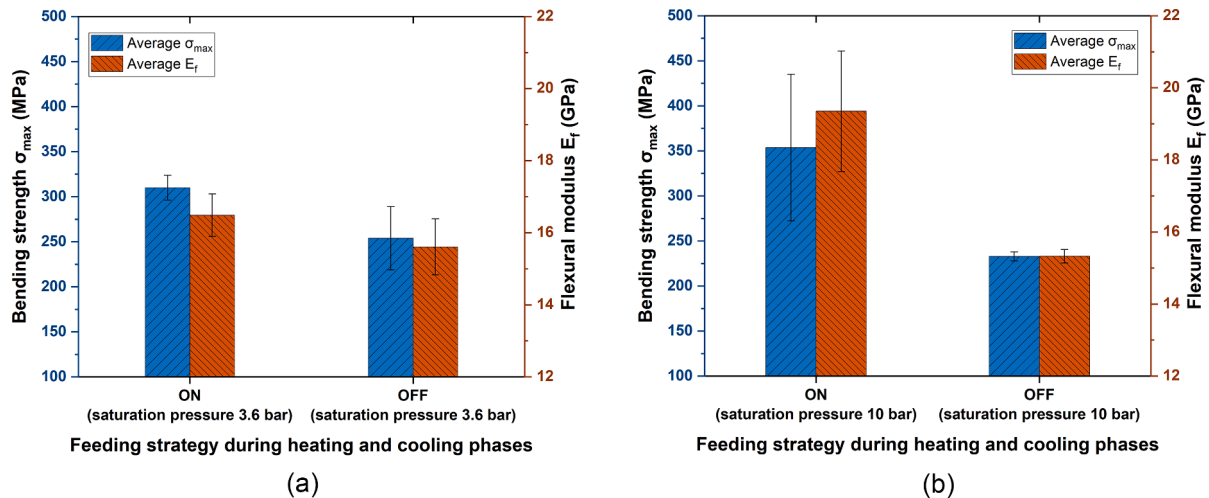


Fig. 14. Bending strength and bending modulus as a function of the feeding strategy; with saturation pressures of 3,6 (a) and 10 (b) bar. (Injection at 240 °C and saturation time of 10 min for all samples).

(45.8%) was used and values for the viscosity of the resin at the different temperatures were taken from the viscosity measurements of HFGA6 presented in Fig. 1. Darcy's law was used to calculate the injection times for the single inlet and double inlet systems while numerical simulations were performed for the peripheral system, using an in-house Control Volume Finite Element (CVFE) flow simulation code, as detailed in [47,48]. In this scenario, we assume a spacer geometry adapted for radial flow that results in a spider web-like distribution and it would result in an isotropic permeability in in-plane directions. The in-plane apparent permeability value was taken to be $1.0 \times 10^{-8} \text{ m}^2$ for an overall fiber volume fraction of 45%.

Injection times, calculated as a function of the temperature and the injection system, are presented in Table. 3. The saturation step, required to improve the transverse impregnation, was not considered, as its duration is assumed to be the same for all the injection systems and for a given part thickness. The longest injection time is obtained with the

single inlet injection system working at 240 °C and was calculated to be 87.1 min. Conversely, when the injection system is optimized, i.e. a peripheral injection, and an injection temperature of 280 °C, to reduce the viscosity of the resin, as well as an adequate spacer material are used, the injection time drops by 92.2%, down to an injection time of 6.8 min. As a result, the entire impregnation process of the part is shortened to about 7–10 min injection plus saturation/spacer collapse time, which reduces labor, energy, plant operating and machine depreciation costs; resulting in a lower total cost, as compared to impregnation with a G-Ply fabric, for example, which would take on the order of 40 min with a double inlet injection system. However, to be able to inject at such temperatures, spacers must be manufactured with polymers with a higher melting point (i.e. above 305–310 °C for injections at 280 °C) and with an adapted channel geometry, for example with a radial pattern of flow channels. High temperature polyamides, like PPA or PA6T/PA6I/PA6, could be injection molded which would ensure short cycle times

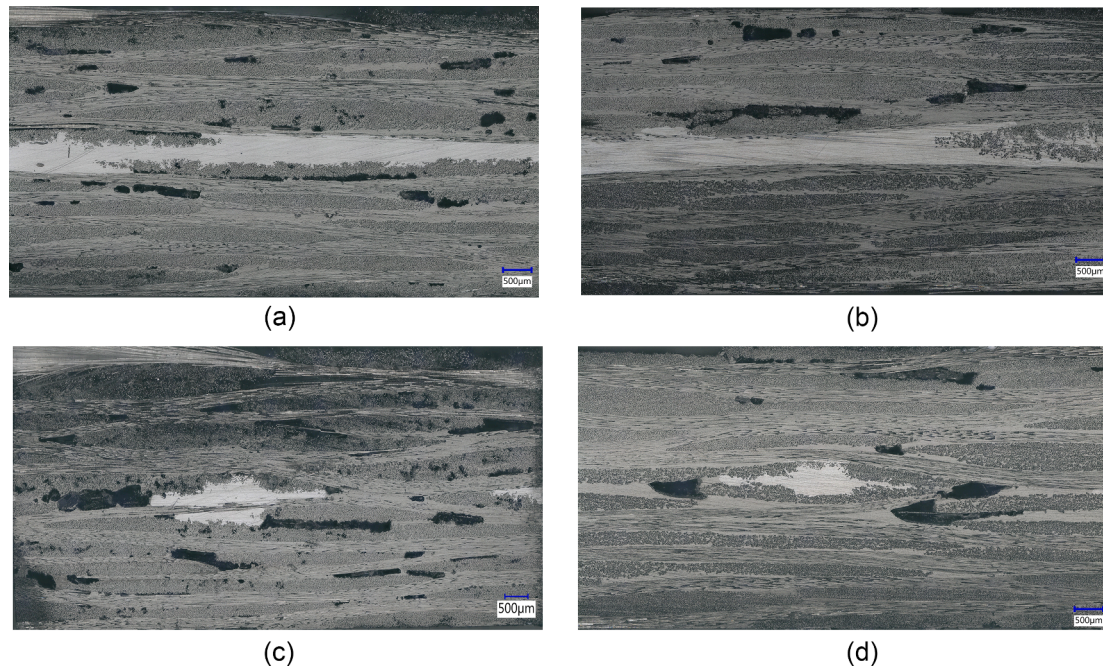


Fig. 15. Optical micrographs of samples cut close to the outlet, longitudinally (a and b) and transversally (c and d) to the resin flow; stopping (a and c) or maintaining (b and d) resin injection during the collapsing phase of the spacer and the cooling of the mold. (Injection at 240 °C/Saturation phase: 10 bar for 10 min).

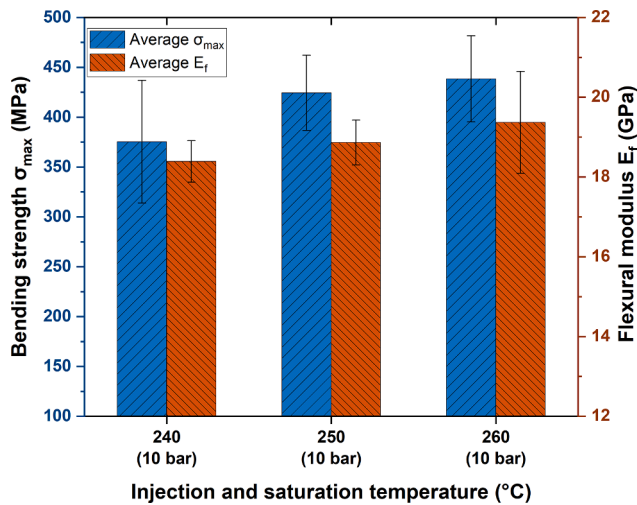


Fig. 16. Bending strength and bending modulus as a function of the injection and saturation temperature. (Saturation phase: 10 bar for 20 min. Feeding ON).

and a good chemical compatibility with the HFGA6 matrix.

Using the mTP-RTM technique with this type of injection system, high temperature polyamides as materials for the spacer and low viscosity polyamides for the matrix, would allow to produce complex shape parts for small to medium sized parts in large production volumes.

4. Conclusions

Several processing strategies were investigated to optimize the impregnation quality of flow enhanced glass fiber preforms via in-plane melt thermoplastic resin transfer molding. In addition to reference specimens produced by G-Weave and G-Ply fabrics, several specimens were produced by integration of a 3D-printed polymer spacer in the lay-up, which remained during impregnation then collapsed after a second temperature dwell. The spacer material choice and design highlighted the needed compromise between the spacer resistance to creep at processing temperature and its ability to melt after a minimal temperature increase. PPS annealed at rather high temperature proved to form an adequate proof-of-concept material.

Several processing parameters were analysed: the saturation pressure, the saturation time, the injection and saturation temperature and the feeding strategy. For each, the effect on bending strength and on porosity content were quantified. Optimal parameters were found, namely by gradually ramping up the applied pressure from 3.6 to 10–15 bars during the saturation phase to ensure full impregnation without creating extensive fiber movement, and keeping polymer feeding during the spacer's collapse temperature dwell and during matrix crystallization in the cool-down phase, to reduce porosity.

For financial and practical reasons, these experiments were all performed at lab scale with a small press and mold instead of a typical injection machine and fine-tuned molds that would be used in industry. Double inlets or peripheral systems could be considered for the injection of larger parts. A simple scale-up analysis of the process was carried out to assess the efficiency of the technique for the production of model automotive parts at large scale. Different injection configurations and

Table 2

Processing parameters and bending properties for samples with the highest impregnation quality.

Plate N°	Saturation time [min]	Saturation pressure [bar]	Temperature [°C]	Feeding	Average σ_{max} [MPa]	Average E_f [GPa]
14	15	10 (10 min) + 15 (5 min)	240	ON	459.8	18.4
16	20	10	260	ON	438.5	19.4
18	20	7 (10 min) + 10 (5 min) + 15 (5 min)	240	ON	471.8	19.0
23	20	10	250	ON	424.6	18.9

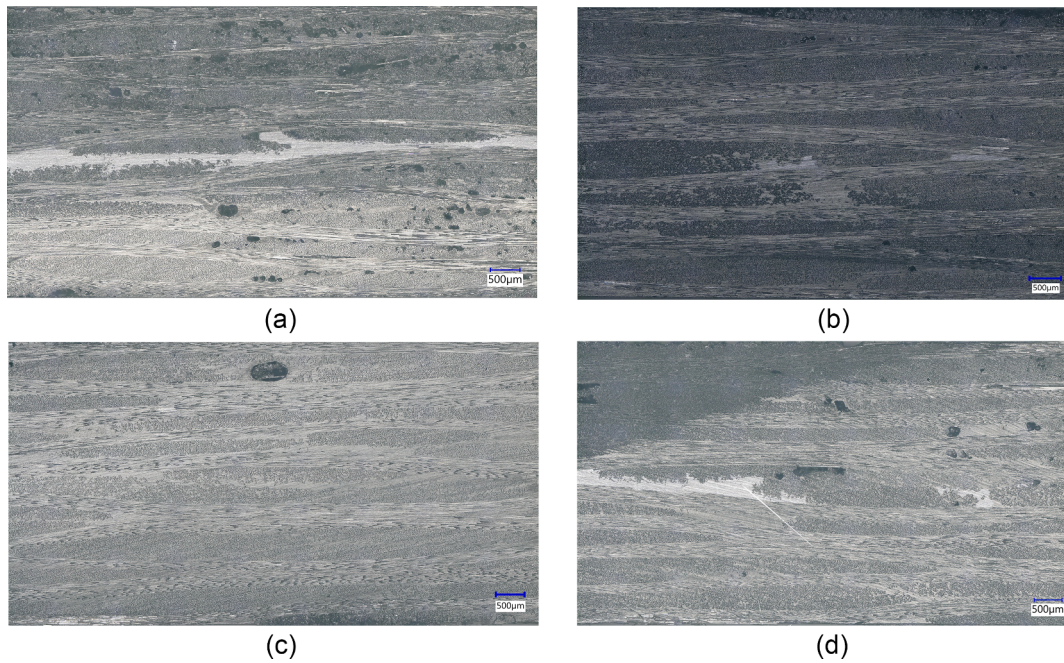


Fig. 17. Micrographs from samples cut close to the outlet on plates n°14 (a), 16 (b), 18 (c) and 23 (d).

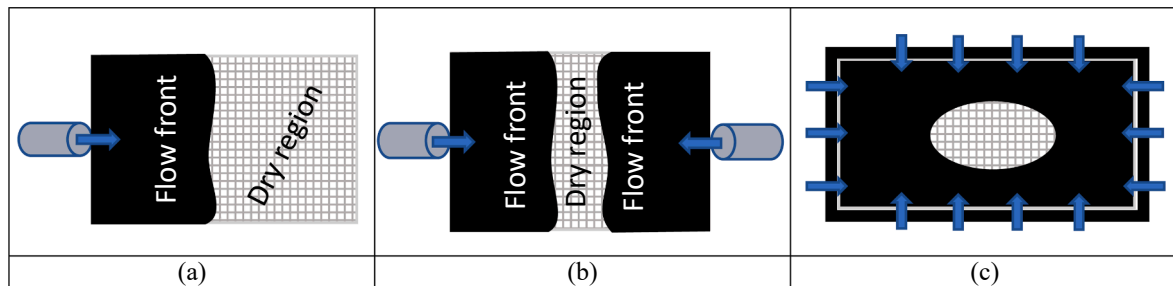


Fig. 18. Injection systems studied for the scale up of the process: single inlet (a), double inlet (b) and peripheral (c).

Table 3

Injection time as a function of the injection system and temperature.

Injection time [min]	Injection method			
	One Inlet	Two Inlets	Peripheral	
Injection and saturation	240	87.1	21.8	13.7
Temperature [°C]	260	61.0	15.3	9.6
	280	43.6	10.9	6.8

temperatures were considered and a peripheral injection system working at 280 °C allowed to reach an injection time of 6.8 min for a 1.5 m × 1.6 m part in dimensions. Together with a saturation time which is only related to part thickness, an overall process time of 10 min could be envisaged, which approaches cycle times required for automotive applications, while allowing one-shot production of parts that may otherwise require several manufacturing steps.

In summary, this process is adapted for complex-shaped parts of limited dimensions. It allows integrating external features and removing welding steps needed for complicated geometries manufactured in metal. Using a flow enhancer designed to manipulate the flow patterns according to the part geometry and integrated to the fabric will enable RTM processes with high fluidity thermoplastics, which were, up to now, discarded at the expense of thermosets for their low viscosity. This technique could also be used in combination with Compression-RTM (C-

RTM), for example for complex parts with a large flat area combined with 3D features benefiting from the presence of a spacer.

CRediT authorship contribution statement

Colin Gomez: Investigation, Methodology, Writing - original draft. **Damiano Salvatori:** Investigation, Methodology, Writing - original draft. **Baris Caglar:** Methodology, Supervision, Formal analysis, Writing - review & editing. **Robin Trigueira:** Investigation, Validation, Writing - review & editing. **Gilles Orange:** Conceptualization, Writing - review & editing. **Véronique Michaud:** Conceptualization, Funding acquisition, Project administration, Supervision, Writing - review & editing.

Declaration of Competing Interest

The authors declare that they have no known competing financial interests or personal relationships that could have appeared to influence the work reported in this paper.

Acknowledgements

The study was funded by the Swiss Competence Center for Energy Research SCCER Mobility of the Swiss Innovation Agency Innosuisse and by Solvay Group (Research Centre of Lyon, France). Chomarat (Le Cheylard, France) is thankfully acknowledged for having provided the

glass fabrics.

References

- van Rijswijk K, Bersee H.E.N. Reactive processing of textile fiber-reinforced thermoplastic composites - an overview. *Compos Part A Appl Sci Manuf* 38 2007 666–81. <https://doi.org/10.1016/j.compositesa.2006.05.007>.
- Parton H, Verpoest I. In situ polymerization of the thermoplastic composites based on cyclic oligomers. *Polym Compos* 2005;26:60–5. <https://doi.org/10.1002/pc.20074>.
- van Rijswijk K, Lindstedt S, Vlasveld DPN, Bersee HEN, Beukers A. Reactive processing of anionic polyamide-6 for application in fiber composites: a comparative study with melt processed polyamides and nanocomposites. *Polym Test* 2006;25:873–87. <https://doi.org/10.1016/j.polymertesting.2006.05.006>.
- van Rijswijk K, Teuwen JJE, Bersee HEN, Beukers A. Textile fiber-reinforced anionic polyamide-6 composites. Part I: The vacuum infusion process. *Compos Part A Appl Sci Manuf* 2009;40:1–10. <https://doi.org/10.1016/j.compositesa.2008.03.018>.
- Vicard C, De Almeida O, Cantarel A, Bernhart G. Experimental study of polymerization and crystallization kinetics of polyamide 6 obtained by anionic ring opening polymerization of ϵ -caprolactam. *Polymer (Guildf)* 2017;132:88–97. <https://doi.org/10.1016/j.polymer.2017.10.039>.
- Li MX, Lee D, Lee GH, Kim SM, Ben G, Il Lee W, et al. Effect of temperature on the mechanical properties and polymerization kinetics of polyamide-6 composites. *Polymers (Basel)* 2020;12:1–20. <https://doi.org/10.3390/POLYM12051133>.
- Murray JJ, Robert C, Gleich K, McCarthy ED, Ó Brádaigh CM. Manufacturing of unidirectional stitched glass fabric reinforced polyamide 6 by thermoplastic resin transfer moulding. *Mater Des* 2020;189. <https://doi.org/10.1016/j.matdes.2020.108512>.
- van Rijswijk K, van Geenen AA, Bersee HEN. Textile fiber-reinforced anionic polyamide-6 composites. Part II: Investigation on interfacial bond formation by short beam shear test. *Compos Part A Appl Sci Manuf* 2009;40:1033–43. <https://doi.org/10.1016/j.compositesa.2009.02.018>.
- van Rijswijk K, Bersee HEN, Beukers A, Picken SJ, van Geenen AA. Optimisation of anionic polyamide-6 for vacuum infusion of thermoplastic composites: Influence of polymerisation temperature on matrix properties. *Polym Test* 2006;25:392–404. <https://doi.org/10.1016/j.polymertesting.2005.11.008>.
- Van Rijswijk K, Bersee HEN, Jager WF, Picken SJ. Optimisation of anionic polyamide-6 for vacuum infusion of thermoplastic composites: choice of activator and initiator. *Compos Part A Appl Sci Manuf* 2006;37:949–56. <https://doi.org/10.1016/j.compositesa.2005.01.023>.
- Teuwen JJE, Van Geenen AA, Bersee HEN. Temperature evolution during processing of thick-walled anionic polyamide 6 composites: experiment and simulation. *Macromol Mater Eng* 2013;298:722–9. <https://doi.org/10.1002/mame.201200083>.
- Yan C, Li H, Zhang X, Zhu Y, Fan X, Yu L. Preparation and properties of continuous glass fiber reinforced anionic polyamide-6 thermoplastic composites. *Mater Des* 2013;46:688–95. <https://doi.org/10.1016/j.matdes.2012.11.034>.
- Maazouz A, Lamnawar K, Dkier M. Chemorheological study and in-situ monitoring of PA6 anionic-ring polymerization for RTM processing control. *Compos Part A Appl Sci Manuf* 2018;107:235–47. <https://doi.org/10.1016/j.compositesa.2018.01.007>.
- Luisier A, Bourbon P, Månson JE. Time – Temperature – Transformation Diagram for Reactive Processing of Polyamide 12 2001;81:963–72.
- Luisier A, Bourbon PE, Månson JAE. Reaction injection pultrusion of PA12 composites: Process and modelling. *Compos Part A Appl Sci Manuf* 2003;34: 583–95. [https://doi.org/10.1016/S1359-835X\(03\)00101-5](https://doi.org/10.1016/S1359-835X(03)00101-5).
- Zingraff L, Michaud V, Bourbon PE, Månson JAE. Resin transfer moulding of anionically polymerised polyamide 12. *Compos Part A Appl Sci Manuf* 2005;36: 1675–86. <https://doi.org/10.1016/j.compositesa.2005.03.023>.
- Wakeman MD, Zingraff L, Bourbon PE, Månson JAE, Blanchard P. Stamp forming of carbon fibre/PA12 composites - A comparison of a reactive impregnation process and a commingled yarn system. *Compos Sci Technol* 2006;66:19–35. <https://doi.org/10.1016/j.compscitech.2005.06.001>.
- Verrey J, Wakeman MD, Michaud V, Månson JAE. Manufacturing cost comparison of thermoplastic and thermoset RTM for an automotive floor pan. *Compos Part A Appl Sci Manuf* 2006;37:9–22. <https://doi.org/10.1016/j.compositesa.2005.05.048>.
- Ó Máirtín P, McDonnell P, Connor MT, Eder R, Ó Brádaigh CM. Process investigation of a liquid PA-12/carbon fibre moulding system. *Compos - Part A Appl Sci Manuf* 2001;32:915–23. [https://doi.org/10.1016/S1359-835X\(01\)00005-7](https://doi.org/10.1016/S1359-835X(01)00005-7).
- Parton H, Baets J, Lipnik P, Goderis B, Devaux J, Verpoest I. Properties of poly (butylene terephthalate) polymerized from cyclic oligomers and its composites. *Polymer (Guildf)* 2005;46:9871–80. <https://doi.org/10.1016/j.polymer.2005.07.082>.
- Mohd Ishak ZA, Leong YW, Steeg M, Karger-Kocsis J. Mechanical properties of woven glass fabric reinforced in situ polymerized poly(butylene terephthalate) composites. *Compos Sci Technol* 2007;67:390–8. <https://doi.org/10.1016/j.compscitech.2006.09.012>.
- Elium® resins for composites 2021. https://www.arkema.com/global/en/products/product-finder/product-range/incubator/elium_resins/. (accessed February 11, 2021).
- Becker D, Francois G, Bozsak V, Mitschang P. Combining the best of two polymer worlds. *Kunststoffe Int* 2016;106:49–51.
- Lin Q, Ferriol M, Cochez M, Vahabi H, Vagner C. Continuous fiber-reinforced thermoplastic composites: influence of processing on fire retardant properties. *Fire Mater* 2017;41:646–53. <https://doi.org/10.1002/fam.2406>.
- Haggi M, El Mahi A, Jendli Z, Akrouf A, Haddar M. Damage Analysis of Flax Fibre/Elium Composite Under Static and Fatigue Testing. In: Haddar M, Chaari F, Benamara A, Chouchane M, Karra C, Aifaoui N, editors. *Des. Model. Mech. Syst.*, Cham: Springer International Publishing; 2018, p. 681–91.
- Obande W, Ray D, Brádaigh Ó, CM.. Viscoelastic and drop-weight impact properties of an acrylic-matrix composite and a conventional thermoset composite – a comparative study. *Mater Lett* 2019;238:38–41. <https://doi.org/10.1016/j.matlet.2018.11.137>.
- Venoor V, Park JH, Kazmer DO, Sobkowicz MJ. Understanding the Effect of Water in Polyamides: A Review. *Polym Rev* 2020:1–49. <https://doi.org/10.1080/15583724.2020.1855196>.
- Orange G, Bessard E, Breard J, Bizet L, Bailleul JL, Comas-Cardona S, et al. Development of composite parts with RTM process based on new high-fluidity thermoplastic polymers. *12th Int Conf Flow Process Compos Mater* 2014:2–3.
- Faraj J, Boyard N, Pignon B, Bailleul JL, Delaunay D, Orange G. Crystallization kinetics of new low viscosity polyamides 66 for thermoplastic composites processing. *Thermochim Acta* 2016;624:27–34. <https://doi.org/10.1016/j.tca.2015.11.025>.
- Faraj J, Pignon B, Boyard N, Bailleul JL, Delaunay D, Orange G. Isothermal crystallization kinetics of low viscosity polyamide 66. *16th Eur Conf Compos Mater ECCM*. 2014 2014..
- Faraj J, Bailleul JL, Boyard N, Delaunay D, Lefevre N, Orange G. Thermal analysis during the consolidation of PA 66 composite by RTM process. *AIP Conf Proc* 2016; 1769.. <https://doi.org/10.1063/1.4963575>.
- Cazaux G, Bizet L, Bréard J, Gomina M, Comas-Cardona S, Binetruy C, et al. Design of a quasi-unidirectional fabric for RTM process with high-fluidity thermoplastic: Longitudinal permeability and microstructure. In: *12th Int Conf Flow Process Compos Mater* 2014.
- Cazaux G. Faisabilité des procédés LCM pour l'élaboration de composites renfort continu à matrice thermoplastique polyamide. 2016.
- Orange G, Maupetit J. Thermoplastic Melt Impregnation of Composite Laminates By Injection- Compression Process. *14th Int Conf Flow Process Compos Mater* 2018.
- Cazaux G, Bizet L, Duchemin B, Moussa G. Surface tension characterization of various polyamides 6,6 for application in RTM process. *Comptes Rendus Des JNC* 2015.
- Salvatori D. Strategies for faster impregnation in melt thermoplastic resin transfer molding process. *Ecole Polytechnique Fédérale de Lausanne* 2018. <https://doi.org/10.5075/epfl-thesis-8763>.
- Studer J, Dransfeld C, Jauregui Cano J, Keller A, Wink M, Masania K, et al. Effect of fabric architecture, compaction and permeability on through thickness thermoplastic melt impregnation. *Compos Part A Appl Sci Manuf* 2019;122:45–53. <https://doi.org/10.1016/j.compositesa.2019.04.008>.
- Orange G, Pascal F, Jaquet P, Giroud A. Process for manufacturing composite articles. *EP 3 572 205 A1*, 2019.
- Cazaux G, Bizet L, Bréard J, Gomina M, Syerko E, Comas-Cardona S, et al. Permeability enhancement with different glass fiber quasi-UD structure arrangements for RTM-TP process. In: *20th Int Conf Compos Mater* 2015.
- Syerko E, Binetruy C, Comas-Cardona S, Leygue A. A numerical approach to design dual-scale porosity composite reinforcements with enhanced permeability. *Mater Des* 2017;131:307–22. <https://doi.org/10.1016/j.matdes.2017.06.035>.
- Salvatori D, Caglar B, Teixidó H, Michaud V. Permeability and capillary effects in a channel-wise non-crimp fabric. *Compos Part A Appl Sci Manuf* 2018;108:41–52. <https://doi.org/10.1016/j.compositesa.2018.02.015>.
- Salvatori D, Caglar B, Michaud V. 3D spacers enhance flow kinetics in resin transfer molding with woven fabrics. *Compos Part A Appl Sci Manuf* 2019;119:206–16. <https://doi.org/10.1016/j.compositesa.2019.01.023>.
- Kracke C, Nonn A, Koch C, Nebe M, Schmidt E, Bickerton S, et al. Interaction of textile variability and flow channel distribution systems on flow front progression in the RTM process. *Compos Part A Appl Sci Manuf* 2018;106:70–81. <https://doi.org/10.1016/j.compositesa.2017.12.010>.
- Palmer RJ. Polyamides, Plastics. *Kirk-Othmer Encycl. Chem. Technol.* 2005. <https://doi.org/10.1002/0471238961.1612011916011213.a01.pub2>.
- Geng P, Zhao J, Wu W, Wang Y, Wang B, Wang S, et al. Effect of thermal processing and heat treatment condition on 3D printing PPS properties. *Polymers (Basel)* 2018;10. <https://doi.org/10.3390/polym10080875>.
- ASTM International. Standard Test Method for Flexural Properties of Polymer Matrix Composite Materials 2007. https://doi.org/10.1520/D7264_D7264M-15.
- Caglar B, Salvatori D, Sozer EM, Michaud V. In-plane permeability distribution mapping of isotropic mats using flow front detection. *Compos Part A Appl Sci Manuf* 2018;113:275–86. <https://doi.org/10.1016/j.compositesa.2018.07.036>.
- Caglar B, Hancioglu M, Sozer EM. Monitoring and modeling of part thickness evolution in vacuum infusion process. *J Compos Mater* 2020. <https://doi.org/10.1177/0021998320963173>.
- Kovacs JG, Solymosy B. Effect of glass bead content and diameter on shrinkage and warpage of injection-molded PA6. *Polym Eng Sci* 2009;49:2218–24.
- Michaud V. A review of non-saturated resin flow in liquid composite moulding processes. *Transp Porous Media* 2016;115:581–601. <https://doi.org/10.1007/s11242-016-0629-7>.
- Caglar B, Tekin C, Karasu F, Michaud V. Assessment of capillary phenomena in liquid composite molding. *Compos Part A Appl Sci Manuf* 2019;120:73–83. <https://doi.org/10.1016/j.compositesa.2019.02.018>.